



DESY
SUMMER STUDENT PROGRAM
2010

Measurement of the $W+\text{jet}/Z+\text{jet}$ crosssection ratio with the ATLAS detector

Author:
Sten Luyckx

Supervisor:
Gerhard Brandt

Abstract

This report describes the measurement of the ratio of $W+\text{jets}$ to $Z+\text{jets}$ cross sections. These measurements are then compared with Next-to-Leading Order (NLO) perturbative theory predictions. For this study ATLAS data is used from $\sqrt{s} = 7$ TeV proton-proton collisions at the LHC corresponding to a total integrated luminosity of approximately 1.45 pb^{-1} .

Contents

1	Introduction	2
2	ATLAS detector	2
3	Data and Monte Carlo	3
3.1	Data Quality	4
3.2	Electron Selection	4
3.3	Jets	6
3.4	Missing transverse energy	6
3.5	Lepton-jet overlap removal	6
3.6	W Selection	6
3.7	Z Selection	6
3.8	Control Plots	6
4	Ratio measurement	11
4.1	Correction to hadron level	11
4.2	Systematic Uncertainties	11
4.3	Ratio	12
5	Summary	13
	Acknowledgments	14
	References	14

1 Introduction

This analysis measures the ratio of the jet production crosssections with associated W/Z production in pp collision at $\sqrt{s} = 7$ TeV. This ratios are robust quantities that do not depend, at first order, on any of the sources of systematic effects which largely affect W+jets and Z+jets cross section measurements (e.g. jet energy scale and resolution effects, modeling of hadronisation and underlying events, etc.). Such ratio measurements therefore constitute powerful analyses to be performed in the early data-taking period of the ATLAS experiment. When measured as a function of the kinematic of the jets in the event, such ratios can be used to:

- perform signature-based, model-independent searches for new physics in final states containing one or two leptons and jets;
- study Next-to-Leading order (NLO) effects on Standard Model (SM) W/Z+jets cross section theoretical predictions;
- obtain data-driven predictions for the irreducible backgrounds contributing to many top, higgs, susy and exotic analyses;
- test lepton efficiency and fake rate estimates in kinematic regions where Monte Carlo haven't been tuned.

In order to reach a sufficiently good sensitivity to such physics perspectives, more than 100 pb^{-1} of ATLAS data are needed. For example, with 10 pb^{-1} of ATLAS data, the statistical uncertainty on Z+1-jet events with a jet of at least 30 GeV of transverse energy is expected to be of about 6%, while it is expected to be of about 15% if the jet is above 75 GeV. This is not enough to find new physics, nor to test SM NLO predictions or lepton efficiency estimates in kinematic regions never probed before. However, this statistical uncertainty is low enough for the ratio to be sensitive to systematic effects on the missing transverse energy (E_T^{miss}) acceptance and on QCD multijet background to W/Z+jets events estimates, in low kinematic regions. With 1 pb^{-1} of data, the statistical uncertainty on the R_{jets} measurements is expected to be between 15% and 20% in both the electron and muon channels. This analyses would therefore only be sensitive to large discrepancies between data and Monte Carlo on the E_T^{miss} acceptance and on the QCD background to W+jets events, if any. It is nevertheless an important milestone in getting toward the realization of the rich physics potential of the R_{jets} analyses at higher luminosity.

In the following, we will therefore present the $R_{1\text{-jet}}$ analysis performed with approximately 1.45 pb^{-1} of data using the electron channel. This means that we only look at events that have 1 jet + W or a Z for the ratio measurement. For the W we only look at the $W \rightarrow e\nu$ and for the Z we only look at the $Z \rightarrow ee$ channel.

2 ATLAS detector

The ATLAS detector [1], shown in figure 1, at the LHC comprises a thin superconducting solenoid surrounding the inner-detector cavity and three large superconducting toroids arranged with an eight-fold azimuthal coil symmetry placed around the calorimeters, forming the basis of the muon spectrometer.

The Inner-Detector (ID) system is immersed in a 2 T axial field and provides tracking information for charged particles in a pseudorapidity range matched by the precision measurements of the electromagnetic calorimeter; the silicon tracking detectors, pixel and silicon microstrip (SCT), cover the pseudorapidity range $|\eta| < 2.5$. The highest granularity is achieved around the vertex region using the pixel detectors. The Transition Radiation Tracker (TRT), which surrounds the silicon detectors, enables track-following up to $|\eta| = 2.0$. Electron identification information of the TRT is provided by the detection of transition radiation in the TRT straw tubes.

The calorimeter system covers the pseudorapidity range $|\eta| < 4.9$, using a variety of detector technologies. The electromagnetic (EM) calorimeter consists of lead absorbers and liquid argon (LAr) as the active material is divided into a barrel part ($|\eta| < 1.475$) and two end-cap components ($1.375 < |\eta| < 3.2$). The pseudorapidity range $1.37 < |\eta| < 1.52$ is considered as the transition region between the barrel and end-cap, where a reliable measurement is not possible, and is omitted

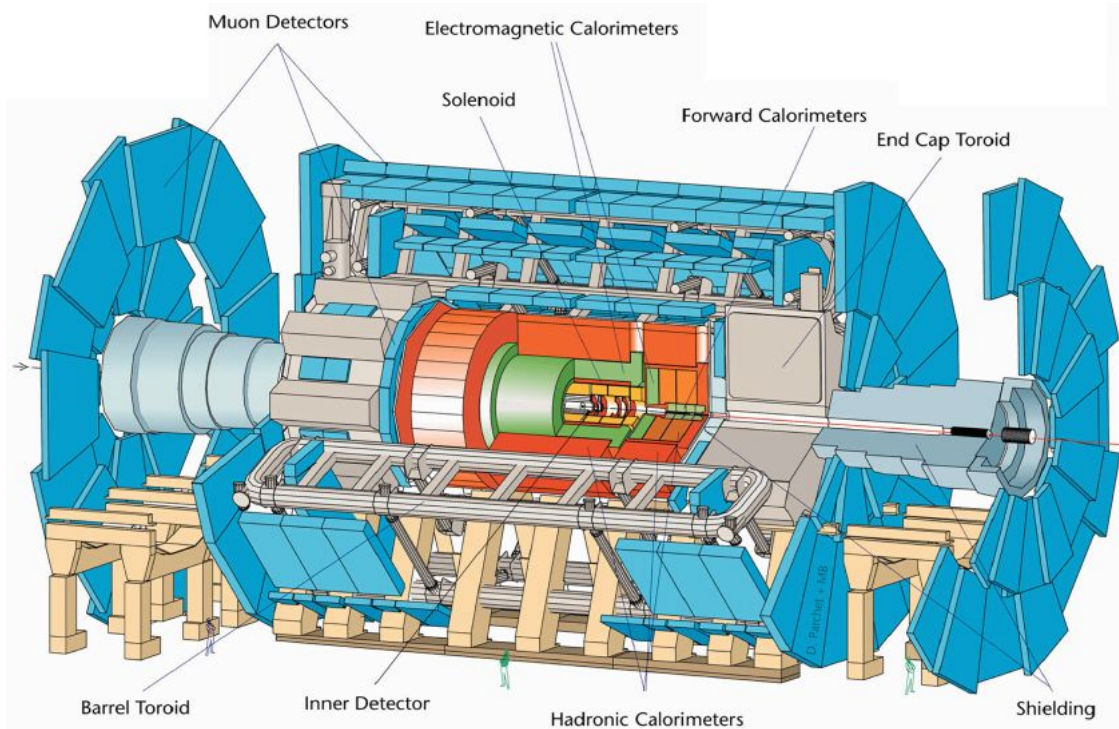


Figure 1: Schematical overview of the ATLAS detector.

for this ratio analysis. In the region of $|\eta| < 1.8$, a presampler detector consisting of a thin layer of LAr is used to correct for the energy lost by electrons, positrons, and photons upstream of the calorimeter. The hadronic tile calorimeter is placed directly outside the EM calorimeter envelope. This steel/scintillating-tile detector consists of a barrel covering the region $|\eta| < 1.0$, and two extended barrels in the range $0.8 < |\eta| < 1.7$. The copper Hadronic End-cap Calorimeter (HEC) which uses LAr as the active material consists of three modules in each end-cap: the first, made of copper, is optimised for electromagnetic measurements, while the other two, made of tungsten, measure primarily the energy of hadronic interactions.

The first-level (L1) trigger system uses a subset of the total detector information to make a decision on whether or not to process an event, reducing the data rate to approximately 75 kHz. The subsequent two levels, collectively known as the high-level trigger, are the Level-2 (L2) trigger and the event filter. They provide the reduction to a final data-taking rate of approximately 200 Hz.

3 Data and Monte Carlo

The data from $\sqrt{s} = 7$ TeV proton-proton collisions at the LHC were used for this analysis. This contains the runs from April 18 2010 to August 18 2010 which are sorted in periods from A till E7 and shown in table 1. This sample corresponds to a total integrated luminosity of 1.4569 pb^{-1} .

During this initial period of detector operation, there have been several trigger and detector changes. However, an important bonus of making a measurement of a cross section ratio is that all changes listed above affect numerator and denominator the same way, hence do not need to be explicitly accounted for in the analysis.

The trigger menu also changed quite a lot, to be able to follow the rapid increase of the LHC instantaneous luminosity which characterized this initial period. Again, the changes in the trigger efficiency cancel out in the ratio. Before these can be used for the ratio measurement, a selection process has to take place. This is covered in the following subsections.

Period	Runs	L (nb ⁻¹)
A	152166–153200	0.4
B	153565–155160	9.0
C	155228–155697, 156682	9.5
D	158045–159224	320
E1	160387–160479	144
E2	160530	96
E3	160613–160879	272
E4	160899–160980	133
E5	161118–161379	138
E6	161407–161520	160
E7	161562–161948	175

Table 1: ATLAS runs processed in this analysis, with their integrated luminosity.

To simulate all the possible decay processes of W and Z, and the background processes, 4 different MC generators are used which are listed briefly below.

- Alpgen[3] + Jimmy + Herwig
for the leptonic decays from W and Z: $W \rightarrow e\nu$, $W \rightarrow \mu\nu$, $W \rightarrow \tau\nu$, $Z \rightarrow ee$, $Z \rightarrow \mu\mu$ and $Z \rightarrow \tau\tau$;
produced together with 0 up to 5 partons:
- MC@NLO + Jimmy + Herwig
for the s and the t channel of single top decay to $e\nu$, $\mu\nu$ and $\tau\nu$
for the decay of $t\bar{t}$
for all the possible leptonic decays of W^+W^- , ZZ , W^-Z and W^+Z
- Sherpa
for the jet decays into $e\nu$, $\mu\nu$, $\tau\nu$, ee , $\mu\mu$ and $\tau\tau$
- Pythia[4]
to simulate the QCD background (dijet production)
for the decays $W \rightarrow e\nu$, $W \rightarrow \mu\nu$, $W \rightarrow \tau\nu$, $Z \rightarrow ee$, $Z \rightarrow \mu\mu$ and $Z \rightarrow \tau\tau$ (as a check for Alpgen)

3.1 Data Quality

A preselection on event level is done to guarantee the data quality. The event first of all needs to be part of the good runlists. The good runlists are based on the global ATLAS sanity flags ATLGL, L1CTP ready and LHC StableBeam. The quality of the electron reconstruction is ensured by requesting the following virtual flags: `cp_eg_electron_barrel` and `cp_eg_electron_endcaps`, as well as `cp_eg_electron_forward` for the Zee-Forward GRL. In addition the primary flag for the calorimeter trigger, L1Calo, is included in the requirements. For the $W \rightarrow e\nu$ list, the `cp_met` flag (a combination of `cp_met_calorimeter` and `cp_met_muon`) is requested.

The second preselection requires an event to have at least one primary reconstructed vertex (with at least 3 tracks) compatible with the beam spot in the bunch crossing; $|z_{vtx}| < 150$ mm.

Next, good events are selected with the hardware-based L1 trigger (L1_EM14). The L1 calorimeter trigger selects photons and electrons within $|\eta| < 2.5$ using calorimeter information with the reduced granularity of trigger towers of dimension $\Delta\eta \times \Delta\phi = 0.1 \times 0.1$. An algorithm scans the trigger towers with a 2-by-2 matrix and searches for a local maximum. Then the energy of the 2 highest towers inside this 2-by-2 matrix are added together. The trigger used in this analysis accepts electron and photon candidates if this sum is above 14 GeV.¹ This principle is shown in figure 2.

3.2 Electron Selection

The ATLAS standard electron/photon reconstruction and identification algorithm [2] is designed to provide various levels of background rejection optimized for high identification efficiencies for calorime-

¹Normally there is also an isolation requirement, but this has not yet been implemented by the trigger group.

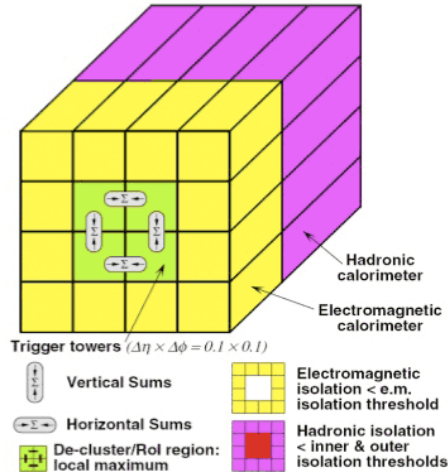


Figure 2: Schematic view of the electromagnetic trigger.

ter transverse energy $E_T > 20$ GeV, over the full acceptance of the inner-detector system. Electron reconstruction begins with a seed cluster of energy of $E_T > 2.5$ GeV in the second layer of the electromagnetic calorimeter. A matching track, extrapolated to the middle EM calorimeter layer, is searched for in a broad window of $\Delta\eta \times \Delta\phi = 0.05 \times 0.1$ amongst all reconstructed tracks with $p_T > 0.5$ GeV. The closest matched track to this layer's cluster barycenter is kept as that belonging to the electron candidate. The final electron candidates have cluster sizes of $\Delta\eta \times \Delta\phi = 0.075 \times 0.175$ in the barrel calorimeter and 0.125×0.125 in the end-cap. The total transverse energy of the clusters is the E_T . Three reference sets of requirements (“loose”, “medium” and “tight”) have been chosen, providing progressively stronger jet rejection at the expense of some identification efficiency loss. Each set adds additional constraints to the previous requirements:

- “loose”: this basic selection uses EM shower shape information from the second layer of the EM calorimeter (lateral shower containment and shower width) and energy leakage into the hadronic calorimeters as discriminant variables. This set of requirements provides high and uniform identification efficiency but a low background rejection;
- “medium”: this selection provides additional hadronic rejection by evaluating the energy deposit patterns in the first layer of the EM calorimeter (the shower width and the ratio of the energy difference associated with the largest and second largest energy deposit over the sum of these energies), track quality variables (number of hits in the pixel and silicon trackers, the transverse impact parameter) and a cluster-track matching variable ($\Delta\eta$ between the cluster and the track extrapolated to the first layer of the EM calorimeter);
- “tight”: this selection further rejects charged hadrons and secondary electrons from conversions by fully exploiting the electron identification potential of the ATLAS detector. It makes requirements on the ratio of cluster energy to track momentum, on the number of this in the TRT, and on the ratio of high-threshold to the total number of hits in the TRT. Electrons from conversions are rejected by requiring at least one hit in the first layer of the pixel detector. A conversion-flagging algorithm is also used to further reduce this contribution. The impact-parameter requirement applied in the medium selection is further tightened at this level.

In the latest version of the analysis, the requirements of medium and tight have been changed to “robustMedium” and “robusterTight”. These changes implicate that, in addition to the regular criteria, electrons are prevented from being flagged as conversions when passing through disabled B-layer modules.

After the electrons have been constructed by this egamma algorithm with option `author` is 1 or 3, some further cuts are applied on electron level. (This implicates that the event is thrown away if zero electrons of the event satisfy the electron selections.) The first electron selection requires $0 < |\eta| < 2.47$ but with the removal of the crack $1.37 < |\eta| < 1.52$ pass through. The next requirement is that the

cluster p_T of the electron is greater than 20 GeV. Then there is an OTX cleaning cut. The quality of the reconstruction of the energy deposited by the electron in the liquid argon calorimeter is assessed, rejecting all the electromagnetic clusters involving any misbehaving region of this detector.

3.3 Jets

Jet candidates are reconstructed by the anti-Kt4 jet algorithm, seeded by topo clusters (the algorithm is called AntiKt4HTopoJets). Jets are required to have a minimum transverse momentum of 20 GeV, and a pseudorapidity of $|\eta| < 2.8$. Jets not fulfilling these requirements are removed from the jet counting.

After the jets are reconstructed “bad” and “ugly” jets are removed. Bad jets are not associated to in-time energy deposits in the calorimeters. A bad jet is recognised if one of the following three jet identification criteria is true: the first $n90 \leq 5$ and $\text{Hecfraction} > 0.8$, the second $|\text{quality}| > 0.8$ or the third $\text{emf} > 0.95$. Ugly jets correspond to real energy depositions in region where the energy measurement is not accurate, e.g. the transition region between barrel and end-cap and problematic calorimeter regions. These jets are defined by two conditions. TileGap3 energy fraction > 0.5 and energy fraction in dead cells that receive a large correction: $\text{BCH_CORR_CELL} > 0.5$.

3.4 Missing transverse energy

Missing transverse energy is taken as the ATLAS standard MET_LocHadTopo algorithm, where MET is reconstructed as a vector sum over topo clusters. The missing E_T needs to be at least bigger than 25 GeV. (This is only applied for the W selection.) Next MET cleaning is applied. The event is rejected if at least one AntiKt4HTopoJet with $p_T > 10$ GeV is a bad jet.

3.5 Lepton-jet overlap removal

Electron candidates are also likely to be reconstructed as jets. This can be inferred from the correlation between the relative transverse momentum with the distance between all jets (without any preselection) and preselected electron candidates. Electron and jet candidates close to each other are likely to have the same magnitude of transverse momentum. This can be interpreted to mean that electron candidates were reconstructed also as jets. To remove this electron-jet overlap we take all jets before any selection and exclude the closest jet if its closer than $\Delta R = \sqrt{\Delta\eta^2 + \Delta\phi^2} < 0.2$ to the selected electron. Afterwards only events which have no jet closer than $\Delta R < 0.6$ are allowed.

3.6 W Selection

A candidate W event is selected by requiring exactly one selected “robustertight” electron and discarding all events that have at least a second “robustmedium” electron to have a $Z \rightarrow ee$ -veto in the $W \rightarrow e\nu$ channel. The candidate W event must also have a missing transverse energy of $E_T^{\text{miss}} > 25$ GeV. The candidate W event is finally accepted if the W transverse mass satisfies $M_T = \sqrt{2p_T^l p_T^\nu (1 - \cos(\phi^l - \phi^\nu))} > 40$ GeV. The most important cut flows for the W selection process are shown in table 2 and 3. The Monte Carlo selection is scaled to the luminosity.

3.7 Z Selection

A candidate Z event is selected by requiring exactly two “robustmedium” selected and oppositely-charged same-flavour lepton with an invariant mass of $71 < M_{\text{inv}} < 111$ GeV. Cut flows for the Z selection process are shown in table 4 and 4. The Monte Carlo selection is again scaled to the luminosity. The QCD numbers are not correct, because this can’t be calculated. That is one of the reasons why this measurement is done.

3.8 Control Plots

Figure 3 shows the m_T distribution after the full selection process is done for W and Z. The p_T distribution of the bosons is also shown in figure 4. All plots show a clear signal over an almost

Dataset	GRL	Trigger	author _e	η_e	p_t^e	MET Clean	OTX Clean	N _{tight} = 1	N _{medium} = 1	E_T^{miss}	m_T
A-E7	144001680	8869661	8801971	3724978	3724492	3530845	16027	15920	4410	4189	
AlpgenWenu	12699	12482	7971	7788	7451	6746	6745	6246	4561	4559	3792
AlpgenWtaunu	12562	12353	1771	1619	1578	992	991	927	150	150	79
AlpgenZee	1238	1220	975	966	945	879	879	846	475	379	7
JF17 QCD	54784552	54098504	8445253	7773447	7672175	3273875	3273600	3069531	11153	11153	186
EWKbkgW	15353	15101	1111	1043	1023	695	694	651	72	71	38

Table 2: W cut flows showing the number of events passing each step of the $W \rightarrow e\nu$ selection process on data and Monte Carlo. The Monte Carlo values are normalized to luminosity.

Dataset	0 jets	1 jet	2 jets	3 jets	> 3 jets
A-E7	3202	715	3202	191	81
AlpgenWenu	3030	537	134	43	
AlpgenZee	6	1	2	1	0
AlpgenWtaunu	67	53	10	2	1
JF17 QCD	87	27	38	16	5
EWKbkgW	28	4	3	4	15

Table 3: Number of jets after a W candidate passed the $W \rightarrow e\nu$ selection process. The Monte Carlo values are normalized to luminosity.

Dataset	GRL	Prim Vtx	Trigger	$> 1 \text{ author}_e$	$> 1 \eta_e$	$> 1 p_t^e$	MET Clean	$> 1 \text{ OTX Clean}$	$N_{robustmedium} = 2$	M^{inv}
A-E7	144001680	118178944	9637785	6245291	6025951	330197	330158	290966	150717	287
AlpgenZee	1238	1238	1220	975	693	627	462	462	393	365
AlpgenWenu	12699	12699	12482	7971	2004	1858	204	204	177	108
AlpgenZtautau	1231	1231	1214	334	201	187	26	26	23	14
JF17 QCD	54784552	54784552	54098504	8445253	5313348	5078278	271608	271591	235196	122655
EWKbkgZ	26684	26684	26240	2548	1146	1092	174	174	153	89

Table 4: First part of Z cut flow showing the number of events passing each step of the $Z \rightarrow ee$ selection process on data and Monte Carlo. The Monte Carlo values are normalized to luminosity.

Dataset	0 jets	1 jet	2 jets	3 jets	$> 3 \text{ jets}$
A-E7	212	55	13	5	2
AlpgenZee	282	219	46	12	3
AlpgenWenu	0.30	0.21	0.06	0.02	0.00
AlpgenZtautau	0.02	0.01	0.01	0.00	0.00
JF17 QCD	0.00	0.00	0.00	0.00	0.00
EWKbkgZ	0.56	0.11	0.10	0.16	0.18

Table 5: Number of jets after a Z candidate passed the $Z \rightarrow ee$ selection process. The Monte Carlo values are normalized to luminosity.

negligible background. In figure 5 the jet production of the W is shown together with the transverse momentum of the leading jet. The same for Z is shown in figure 6. In figure 3b and 6b the data of the W looks to be shifted from the Monte Carlo. This shift is also independently found in the Z group and is still under investigation.

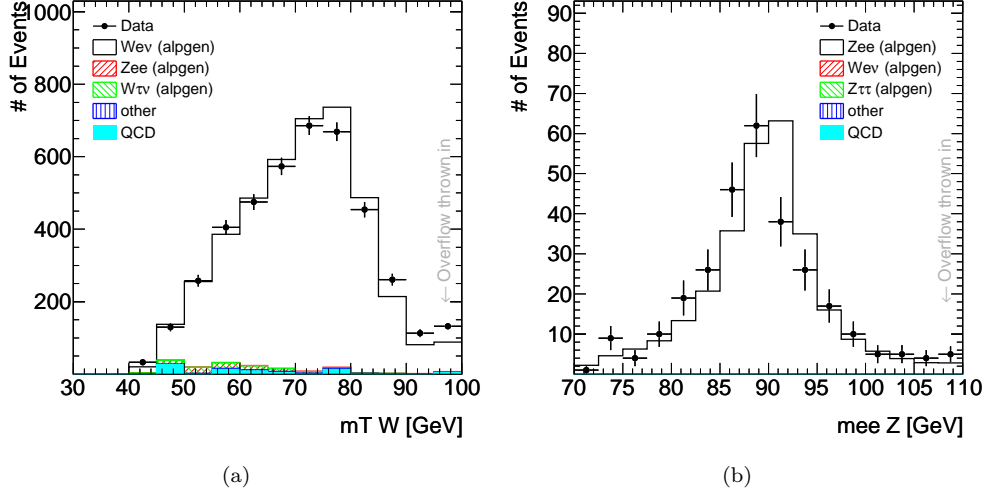


Figure 3: m_T of the W candidates (a) and Z candidates (b) after their full selection.

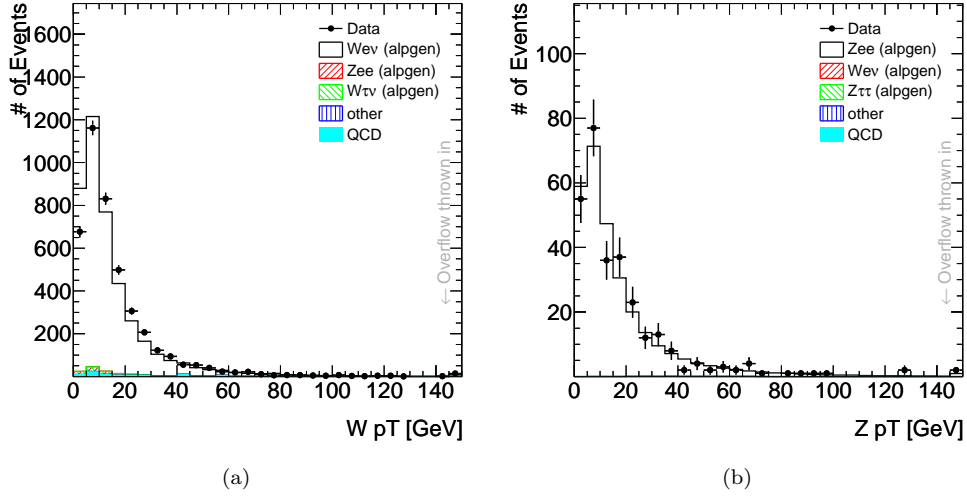
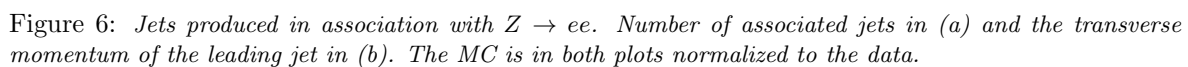
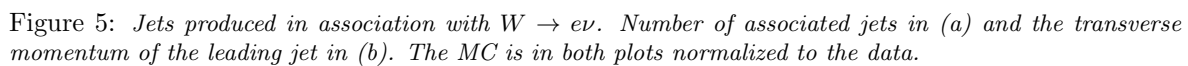


Figure 4: p_T of the W candidates (a) and Z candidates (b) after their full selection.



4 Ratio measurement

4.1 Correction to hadron level

Before the ratio can be calculated, the data needs to be corrected back to the hadron level. The master formula to get the corrected number N_V of one kind of vector boson is:

$$N_V = \frac{(N_{data} - N_{QCD})(1 - f_{ewk})}{(A \times \epsilon) \cdot L} \quad (1)$$

with:

- N_{data} The selected events
- N_{QCD} QCD background fitted
- f_{ewk} Fraction of electroweak background (MC)
- $A \times \epsilon$ Acceptance.Efficiency
- L Luminosity

The QCD fraction is fitted in $p_{T,jet}$ bins to the data. N_{QCD} can be exchanged by $f_{QCD} \times N_{data}$ with f_{QCD} the QCD fraction of the data. Keep in mind that all the corrections for $A \times \epsilon$ need to be done in consistent phase space.

$$A \times \epsilon = (A \times \epsilon)_{jet} \cdot A_{MET|jet} \cdot (A \times \epsilon)_{lepton|jet+MET} \quad (2)$$

The first term describes the correction for the jets. This factor and the Luminosity will cancel out when we calculate the W/Z ratio. The second term describes the acceptance of the missing E_T after the jet cut in every njet bin. The last term in the formula describes the lepton acceptance and efficiency applying the missing E_T and the jet cut. This term contains an acceptance of an object consisting of a cluster matched to a track in our phase space and the electron identification efficiency for such objects. The electron ID efficiency was estimated with Monte Carlo. This was done with a single electron efficiency binned in η and E_T .

To get the correct statistical error, 10000 pseudo experiments using poisson variations are done for the (not acumulated) jet p_T spectrum and afterwards the bins were acumulated to get the cumulative jet p_T distribution. The variation of the corrected R_{jet} was used to estimate the statistical error.

4.2 Systematic Uncertainties

For the systematics uncertainties that are combined up so far²:

- The scaling factor of the QCD background fraction was varied. This was done inside the fit error of the scaling factor.
- For the electroweak background, the effect of the use of pythia instead of alpgen was used. Additionally the uncertainties of the measured quantities were estimated by comparing a selection using truth electron η , p_T and MET instead of the measured electrons.
- The uncertainty concerning the electron ID was estimated using medium electrons instead of tight electrons for the W.
- For the electron acceptance, the scale uncertainty and the difference between alpgen and pythia was taken into account.
- For the electron efficiency the uncertainty estimated by the ID group was used and the correlated part between the W and Z efficiency was removed.

²At the time of this report, people are still finishing the study of the systematical error.

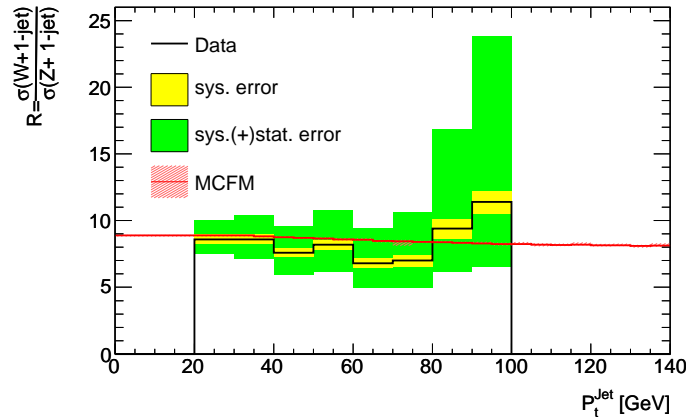


Figure 7: R_{1-jet} in function of the transversal jet energy P_T^{jet} is shown for the electron channel. The theoretical prediction is showed in green, the measurement is displayed in black with the error in red.

Then, the correlation on the single electron efficiency between W and Z is very big, because the Z decays into two electrons and a W into one electron. This results in the 5% uncertainty on efficiency. So most of the systematics count twice in case of the Z. The dependency of the number of jets on the different η distributions due to different selection cuts in W and Z is small in comparison to this error. The systematics of the backgrounds only slightly change the error, because only the weighting of the different bins for the average efficiency is affected.

4.3 Ratio

Now the ratio

$$R_{1-jet} = \frac{\sigma(W + 1 - jet)}{\sigma(Z + 1 - jet)}$$

can be calculated and compared to theoretical predictions. The ratio is plotted in function of a jet kinematic value, in this case the transverse jet energy. This is shown in figure 7. The result is plotted in black, with the statistical poisson 80% error interval in green. (When there is more data available, this error will become gaussian. and the error would correspond with 1σ .) Then in yellow the systematic uncertainties are plotted and in red the theoretical MCFM prediction. This theoretical prediction is calculated with the use of MCFM (Monte Carlo for FeMtobarn processes). MCFM is a parton-level Monte Carlo generator. Some extra corrections to MCFM are needed to correct for non-perturbative effects affecting the jets.

The result shows an agreement of the calculated ratio and the MCFM theory, but this is mainly due to the fact that the statistical error is still very large. To get a nice clean measurement, 100 pb^{-1} of data is needed, like it was mentioned in the introduction of this report.

A figure of the different contributions of the systematics (not all, only the ones that are already calculated) is plotted in figure 8.

5 Summary

This report covered the 1.45 pb^{-1} analysis of the measurement of the $\frac{\sigma(W+1\text{-jet})}{\sigma(Z+1\text{-jet})}$ cross section ratio with the ATLAS detector by using $\sqrt{s} = 7 \text{ GeV}$ proton proton collisions at the LHC.

For this analysis all data from April 18 till August 18 was used. After the full selection, 4189 W and 287 Z candidates were acquired. Some control plots of the W and Z candidates were shown and they all have a low background.

Before the cross section ratio can be calculated, a correction was done to get back to the hadron level. This incorporates the single electron acceptance and efficiency. Finally the ratio has been calculated and compared to the theoretical prediction of MCFM, a parton level Monte Carlo simulator. The result of the ratio $R_{1\text{-jet}} = \frac{\sigma(W+1\text{-jet})}{\sigma(Z+1\text{-jet})} = 8.8 \pm 1.2$ at $p_T^{\text{jet}} = 20 \text{ GeV}$ agrees with the theoretical prediction, but the statistical error is very big. This analysis will have to be redone with approximately 100 pb^{-1} to get a nice result.

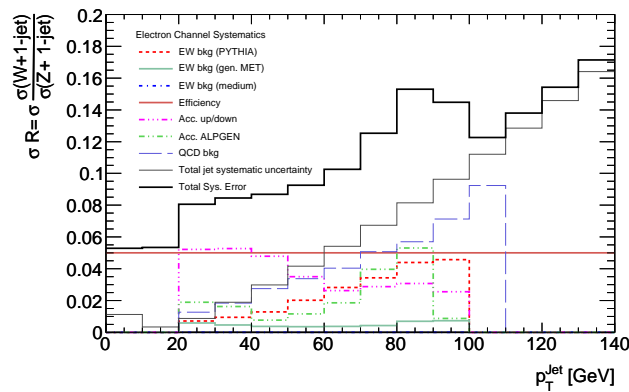


Figure 8: $R_{1\text{-jet}}$ in function of the transversal jet energy p_T^{jet} is shown for the electron channel. The different kind of systematic contributions are shown here. With the total systematic contribution in black calculated by adding the contributions in quadrature. Note, not all systematics have been included in this figure.

Acknowledgments

I would like to thank DESY to make it possible, for us undergraduate students, to participate in a Summer Student Program. A program like this, is a great way to explore and get introduced in the day-to-day work of a physicist. It is also a perfect opportunity to learn to work together and to communicate with other people to accomplish a certain goal. For this reason, I would like to thank all the people who are involved in the organisation of this wonderful program and in special Joachim Meyer.

Then I would like to express my gratitude to my supervisor, Gerhard Brandt, whose expertise, understanding, and patience, added considerably to my experience. Thanks for everything !

Last but not least, I would like to thank the other Summer Students, who all together made this an excellent, once in a lifetime, experience.

References

- [1] The ATLAS Collaboration, G. Aad et al., *The ATLAS Experiment at the CERN Large Hadron Collider*, JINST **3** (2008) S08003
- [2] The ATLAS Collaboration, G. Aad et al., *Electron and photon reconstruction and identification in ATLAS: expected performance at high energy and results at $\sqrt{s}=900$ GeV*, ATLAS conference note: ATLAS-CONF-2010-005
- [3] M. L. Mangano, M. Moretti, F. Piccinini, R. Pittau and A. D. Polosa, *ALPGEN, a generator for hard multiparton processes in hadronic collisions*, JHEP **0307**, 001 (2003) [arXiv:hep-ph/0206293]
- [4] T. Sjostrand, P. Eden, C. Friberg, L. Lonnblad, G. Miu, S. Mrenna and E. Norrbin, *High-energy physics event generation with PYTHIA 6.1*, Comput. Phys. Commun. **135**, 238 (2001) [arXiv:hep-ph/0010017]